Biosensors and Bioelectronics 190 (2021) 113376

Contents lists available at ScienceDirect

Biosensors and Bioelectronics

journal homepage: www.elsevier.com/locate/bios

SPR/SERS dual-mode plasmonic biosensor via catalytic hairpin assembly-induced AuNP network

Chunyuan Song, Jingjing Zhang, Xinyu Jiang, Hongyu Gan, Yunfeng Zhu, Qian Peng, Xinyue Fang, Yan Guo, Lianhui Wang *

State Key Laboratory for Organic Electronics and Information Displays & Jiangsu Key Laboratory for Biosensors, Institute of Advanced Materials (IAM), Jiangsu National Synergistic Innovation Center for Advanced Materials (SICAM), Nanjing University of Posts and Telecommunications, Nanjing, 210023, China

ARTICLE INFO

Keywords:
Surface plasmon resonance
Surface-enhanced Raman scattering
Dark-field imaging
Dual-mode
Plasmonic biosensor
Catalytic hairpin assembly
AuNP network

ABSTRACT

Highly sensitive and reliable detection of disease-related nucleic acids is still a big challenge in liquid biopsy because of their homologous sequences and low abundance. Herein, a novel surface plasmon resonance/surface-enhanced Raman scattering (SPR/SERS) dual-mode plasmonic biosensor based on catalytic hairpin assembly (CHA)-induced Au nanoparticle (AuNP) network was proposed for highly sensitive and reliable detection of cancer-related miRNA-652. The biosensor includes capture DNA-functionalized AuNPs (Probe 1), H1 and 4-mercaptobenzoic acid (4-MBA) co-modified AuNPs (Probe 2), and 6-carboxyl-Xrhodamine (ROX)-labeled H2 (fuel strands). The Probe 1-Probe 2 networks were formed via the target-triggered CHA reactions, which resulted in the color change of dark-field microscopy (DFM) images and enhanced SERS effect. The SPR sensing was achieved by extracting the integral optical density of dark-field color in DFM images, and the SERS sensing was realized by the ratiometric SERS signals of ROX and internal standards 4-MBA molecules. After characterizing the feasibility and optimality of the sensing strategy, the good performance of biosensors on sensitivity, specificity and uniformity was approved. The practicability of biosensors was confirmed by detecting miRNA-652 in human serum, and both the SPR and SERS assays showed good linear calibration curves and low limit of detections (LODs) of 42.5 fM and 2.91 fM, respectively, with the recovery in the range of 94.67–111.4%. These two modes show complementary advantages, and the combined SPR/SERS dual-mode can provide more options for detection and double check the results to improve the accuracy and reliability of assays, which holds a great application prospect for cancer-related nucleic acids detection in early disease stage.

1. Introduction

The accurate detection of trace nucleic acids is crucially important for the reliable analyses of diseases related biomarkers in the early diseases stage and plays significant roles in disease diagnosis, treatment, and pathogenesis (Graybill and Bailey, 2016; van Rooij and Olson, 2012; Zhao et al., 2015). However, genetic variation resulting from some subtle changes of nucleic acid sequence can bring out significant biological influence (Sauna and Kimchi-Sarfaty, 2011). Therefore, developing ultrasensitive and reliable methodologies for the detection of low-abundance disease-related biomarkers is fundamentally important and is becoming an unstoppable trend. Traditional analytical methods, such as northern blotting (Schwarzkopf and Pierce, 2016), microarray technology (Taniguchi et al., 2001), and real-time quantitative polymerase chain reaction (PCR) (Mocellin et al., 2003; Shu et al., 2017), are widely applicable to nucleic acids detection. Besides these traditional methods, various optical and electrical biosensors have been utilized toward the detection of nucleic acids by coupling with different nanomaterials or signal amplification strategies (Chen et al., 2018; Wu et al., 2020). Because of the low abundance of nucleic acid markers in early stage of disease and the complex composition of the sample, single mode detection is vulnerable to missed diagnosis or diagnostic errors. Therefore, it is strongly desirable to develop multi-mode assays for nucleic acids detection to improve the sensitivity and specificity (Wang et al., 2021; Xue et al., 2020).

Recently, plasmon based sensing technologies such as surface plasmon resonance (SPR) (Nguyen et al., 2015; Singh, 2016; Zhang et al., 2018) and surface-enhanced Raman scattering (SERS) (Wang et al., 2013; Zhang et al., 2019, 2020; Zong et al., 2018) have been attracted extensive research attention since they could offer highly sensitive,

* Corresponding author.
E-mail address: iamlhwang@njupt.edu.cn (L. Wang).

https://doi.org/10.1016/j.bios.2021.113376
Received 18 February 2021; Received in revised form 25 April 2021; Accepted 21 May 2021
Available online 29 May 2021

label-free detections with small amount, low cost and simple setup. Up to now, many efforts have been made to design the superior plasmonic nanostructures or improve the bioactivity of the nanointerface modified with biomolecules to achieve higher sensitivity based on single mode detections. However, with the improved sensitivity, the reliability of the sensor could be sacrificed since the exceptional sensitivity is very vulnerable to high background spectral signals from contaminations or from other analytes in the complex samples. This problem not only jeopardizes the true sensitivity for detecting the targeted analyte with the increasing chances to produce false positive or false negative signals, but also creates issues in practical application. An optimal strategy to improve the reliability of highly sensitive sensor is the development of two-in-one (SPR and SERS) sensor, i.e., use more than one sensor to detect the same targeted analyte, which is expected to simultaneously coordinate their respective advantages and compensate each other's shortcomings to achieve an accurate and reliable detection. However, since the SERS enhancement mainly relies on the excitation of localized surface plasmons (LSPs) (Hossain et al., 2008; Lee et al., 2011, 2018), while the SPR is based on the propagating surface plasmon polaritons (SPP), the sensing principles for SERS and SPR are very different and the combination of SPR and SERS detection strategy (SPR/SERS) has seldom been used in plasmonic sensors (Dyankov et al., 2012; Guo et al., 2008; Potara et al., 2011). Thus, it is very challenge to develop SPR/SERS dual-mode sensor (Lee et al., 2018). In our recent work, we reported a robust SERS/SPR dual-mode biosensor prepared on a silver nanorod-covered silver nanohole (Ag NR-NH) array which possessed excellent anisotropic extraordinary optical transmission and strong localized surface plasmon resonance with good SPR response and excellent SERS activity (Song et al., 2020). The Ag NR-NH array was prepared by nanosphere lithography (NSL), reactive ion etching (RIE), physical evaporation deposition, and oblique angle deposition (OAD), which relatively has higher requirements for instrument and procedures. The construction of SPR/SERS dual-mode sensor and its sensing strategy based on colloidal nanoparticles is expected to make the preparation and application of the sensor more convenient. However, the design and development of colloidal nanoparticles-based higher sensitive and reliable SPR/SERS dual-mode biosensors by controllable assembly of nanoparticles with drastically enhanced SERS-active hot spots and uniform SERS signal are still big challenges.

Herein, a highly sensitive and reliable SPR/SERS dual-mode plasmonic biosensor based on colloidal gold nanoparticles (AuNPs) was proposed with a special designed catalytic hairpin assembly (CHA)-induced AuNP network sensing strategy for detecting gastric cancer-related miRNA-652. Two nanoprobes (i.e., capture DNA-functionalized AuNP (Probe 1), and H1 and 4-mercaptobenzoic acid (4-MBA) co-modified AuNP (Probe 2)) were prepared first and with the help of fuel hairpin (6-carboxyl-X-rhodamine (ROX)-labeled H2) target-triggered CHA reactions were executed to induce the formation of Probe 1-Probe 2 networked structures, which resulted in the cycle amplifications, color changes of dark-field microscopy (DFM) images and the enhancement of SERS. The SPR sensing mode was achieved by extracting the integral optical density (IOD) of dark-field color in the DFM images, and the SERS sensing mode was realized by the credible ratiometric SERS signals of ROX molecules and the internal standards 4-MBA. The SERS sensing mode has better sensitivity, while the SPR sensing mode is more available and convenient. These two sensing modes show complementary advantages, and the combined dual-mode sensing can provide more options for detection and double check the results to improve the accuracy and reliability of the biosensor.

2. Mechanism of the SPR/SERS dual-mode sensing

Recently, a novel dark-field microscopy-based SPR measurement based on the IOD of dark-field color in DFM images was reported to not only efficiently determine the abundance of target in the detection system, but also improve the sensitivity of the visual SPR assay (Li et al., 2017, 2018a, 2018b). Besides, the AuNP networked structures with rich nanogaps are considered to have abundant "hot spot" for SERS. However, there is a deficiency that uneven aggregation (i.e., uneven distribution of hot spots) can cause serious nonuniformity in SERS signals. According to this problem, the ratiometric sensing was reported as effective strategy to overcome the instability and achieve the reliable detections (Chen et al., 2019; He et al., 2019; Luo et al., 2020). Therefore, the idea of this work is to design a special sensing strategy (i.e., targeted-induced AuNP network) with observable dark-field color and ratiometric SERS signal based on the AuNP network.

Fig. 1 shows the schematic diagram of SPR/SERS dual-mode plasmonic biosensor based on the CHA-induced AuNP network for the detection of miRNA-652. As shown in Fig. 1a, the AuNP–C probes (Probe 1) are prepared by immobilizing capture DNAs (C) on the surface of AuNPs by Au–S covalent bonds and the AuNP–H1@4-MBA probes (Probe 2) are obtained by immobilizing hairpin DNA H1 (H1) and 4-MBA on the surface of AuNP in sequence. In the presence of target miRNA-652 (T), the H1 hairpins on Probes 2 are opened by the trigger of target to form the T-H1 complex. With the aid of ROX-labeled hairpin DNAs H2 (H2), the T-H1 complexes are triggered to undergo CHA amplification reactions to form numbers of ROX-labeled H1–H2 duplexes on the surface of Probes 2 (Probe 2-CHA), accompanied by the release of miRNA-652 for repeated use. When the H2 hairpins and Probes 1 are added in the above solution, the capture DNAs (C) on the Probe 1 hybridize with the sticky-ends of the H1–H2 duplexes to form the Probe 1-Probe 2 networked structures (Fig. 1b). The formation of Probe 1-Probe 2 network resultes in the color changes of DFM images and the enhancement of SERS. In this case, the DFM image of the Probe 1-Probe 2 network structures on ITO glass scattering yellow or red light can be recorded by a dark-field microscopy. Meanwhile, the SERS assays can be achieved by detecting the SERS signals of ROX and 4-MBA which are strongly enhanced by the rich nanogaps (i.e., hot spots) in the networked structures. In contrast, in the absence of miRNA-652 (T), the mixture of Probes 1 and Probes 2 cannot form the AuNP networked aggregates. Due to the smaller size of AuNPs (15 nm in diameter), the scattered light of individual Probe 1 and Probe 2 on ITO glass is difficult to be observed under the dark-field microscopy, and the relatively isolated AuNPs without remarkable SERS-active hot spots generate very weak Raman signals. The SPR sensing mode can be achieved by extracting the IOD of dark-field color in the DFM images, and the SERS sensing mode is realized by the ratiometric SERS signals of ROX molecules and the internal standards 4-MBA molecules. The preparation of probes, sensing protocol and the SPR/SERS measurements are listed in the experimental sections in the supplementary information (SI).

3. Results and discussion

3.1. Electrophoresis characterization of the sensing mechanism

The feasibility of the CHA and the further hybridization of CHA products with capture DNA (C) were characterized by 10% native-PAGE. As shown in Fig. 2, the lanes 1 to 4 indicate T, H1, H2 and C, respectively. The mixture of H1 and H2 shows two bright bands (lane 9), which is consistent with the positions of H1 and H2. With the aid of miRNA-652 (T), the mixture of T, H1 and H2 in lane 5 shows a new band of CHA products, and a very light band of T can also be observed, which indicates the successful target-triggered CHA amplification. As the concentration of T decreases, the new band gradually becomes lighter (lanes 6–7), illustrating the success of CHA process. In lane 8, after the capture DNA (C) was introduced, a slowly moving band appears, which means the hybridization of CHA products with C. Moreover, H2+C (lane 10), H1+C (lane 11), T + C (lane 12), and H2+T (lane 13) show little change of the band position relative to the ones of individual stripes shown in lanes 1 to 4. Therefore, the PAGE results demonstrate the feasibility of the designed CHA strategy, and the CHA products can effectively recognize the C.

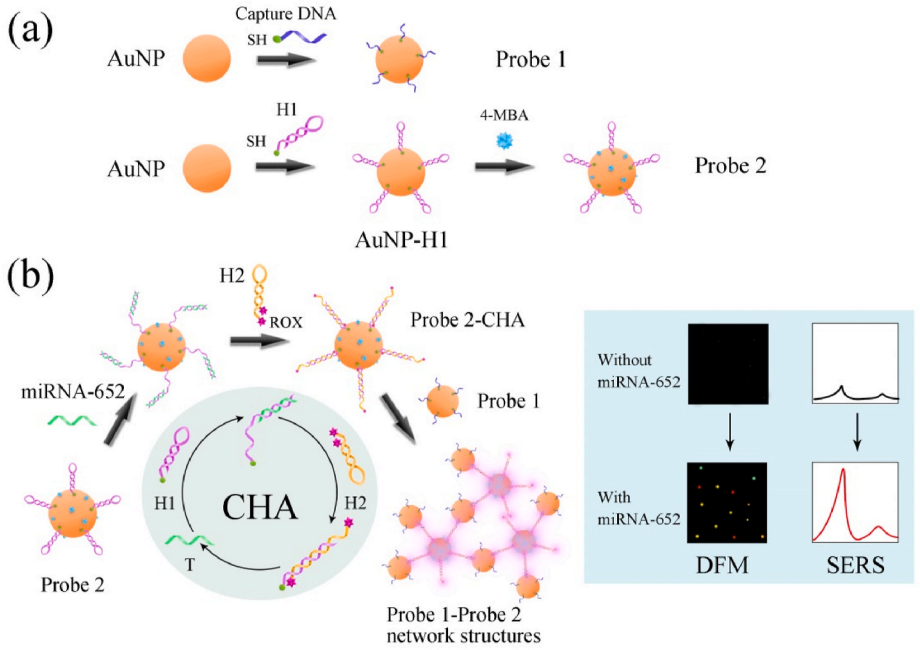

Fig. 1. Schematic diagram of SPR/SERS dual-mode plasmonic biosensor based on CHA-induced AuNP network for the detection of miRNA-652. (a) Preparation of the Probe 1 and Probe 2. (b) SPR/SERS dual-mode sensing strategy based on the CHA-induced AuNP network.

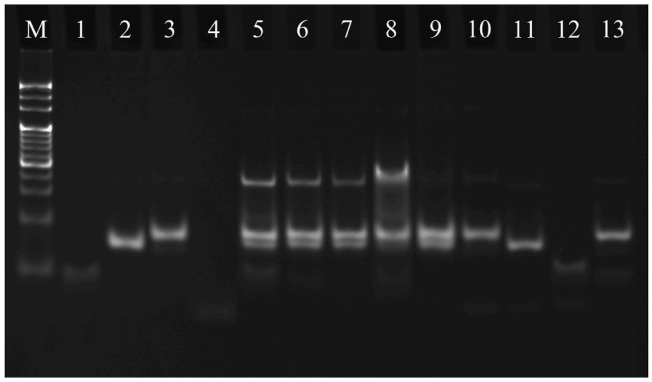

Fig. 2. 10% native-PAGE characterization of the CHA process and hybridization of CHA products with capture DNA (C). Marker (20–500 bp), lane 1: T, lane 2: H1, lane 3: H2, lane 4: C, lane 5: H1+H2+T (1 time), lane 6: H1+H2+T (0.5 times), lane 7: H1+H2+T (0.1 times), lane 8: H1+H2+T+C, lane 9: H1+H2, lane 10: H2+C, lane 11: H1+C, lane 12: T+C, lane 13: H2+T.

3.2. Absorption and morphology characterizations of nanoprobes and networked AuNP

In order to verify the construction of nanoprobes and the feasibility of SPR/SERS dual-mode sensing strategy based on target-triggered CHA-induced AuNP network, absorption spectra and morphology characterizations of the products were recorded (S2.1 in SI), and the results (Figs. S2–3) confirm that the nanoprobes are successfully constructed and the sensing strategy based on target-triggered CHA can effectively induce networked AuNP aggregation.

3.3. Feasibility of SPR sensing by dark-field imaging

Fig. 3 shows the DFM and SEM images of AuNPs, Probe 2, blank control, and the 1 μM miRNA-652 induced Probe 1-Probe 2 networked structures. The scattered light of AuNPs on ITO slide was not observed under the dark-field microscopy (Fig. 3a) due to the small size (15 nm in diameter) of AuNPs (Fig. 3e). After the modifications of H1 and 4-MBA molecules, the scattered light (Fig. 3b) and distribution (Fig. 3f) of Probe 2 have little change compared with the bare AuNPs. DFM image of blank control (i.e., the mixture of Probe 1, Probe 2 and H2) shows few yellow spots (Fig. 3c), and the corresponding SEM image (Fig. 3g) presents a very small amount of AuNP aggregates. The DFM image (Fig. 3d) of specific assay of miRNA-652, i.e., Probe 1-Probe 2 networked structures, displays numerous yellow spots, which suggestes that the SPR measurements based on the sensing strategy of target-triggered CHA-induced AuNP networked aggregation can be successfully executed.

3.4. Feasibility of ratiometric SERS measurements

In order to prepare optimal ratiometric SERS probe, different molar ratios of ROX to 4-MBA, including 1:0.01, 1:0.1, 1:1, and 1:10, were studied by changing the added amount of 4-MBA in the step of preparation of AuNP–H1@4-MBA probes (Probe 2). Fig. 3i shows the schematic diagram of the ratiometric SERS nanoprobe (Probe 2) prepared by co-immobilizing ROX-labeled hairpin DNAs H1 (H1) and 4-MBA molecules (as internal standards) on an AuNP. Fig. 3j shows the SERS responses of the Probe 2 prepared by different molar ratios of ROX to 4-MBA. To clearly show the SERS signal, the SERS spectra were normalized according to the highest intensities at 1500 cm^{-1} (Fig. 3k). Two separated characteristic peaks of ROX at 1500 cm^{-1} and 4-MBA at 1580 cm^{-1} can be observed clearly, and the SERS intensity ratio of ROX to 4-MBA (I_R=I_{1500}/I_{1580}) increased gradually with the increasing relative concentration of ROX (Figure 3l), which indicates that the Probe 2 can effectively output ratiometric SERS signals. Moreover, the optimal molar ratio of ROX to 4-MBA is selected to 1:1 as the characteristic peaks of ROX and 4-MBA are clearly presented with appropriate signal intensity. The superiority of the ratiometric SERS probes were investigated (S2.2 in SI), and the results (Figs. S4–6) indicate that the ratiometric SERS probes can effectively avoid signal fluctuations caused by different detection conditions, and improve the reliability of SERS sensing.

3.5. Optimization of sensing strategy

Dosage ratio of Probe 1 and Probe 2. The dosage ratio of Probe 1 to

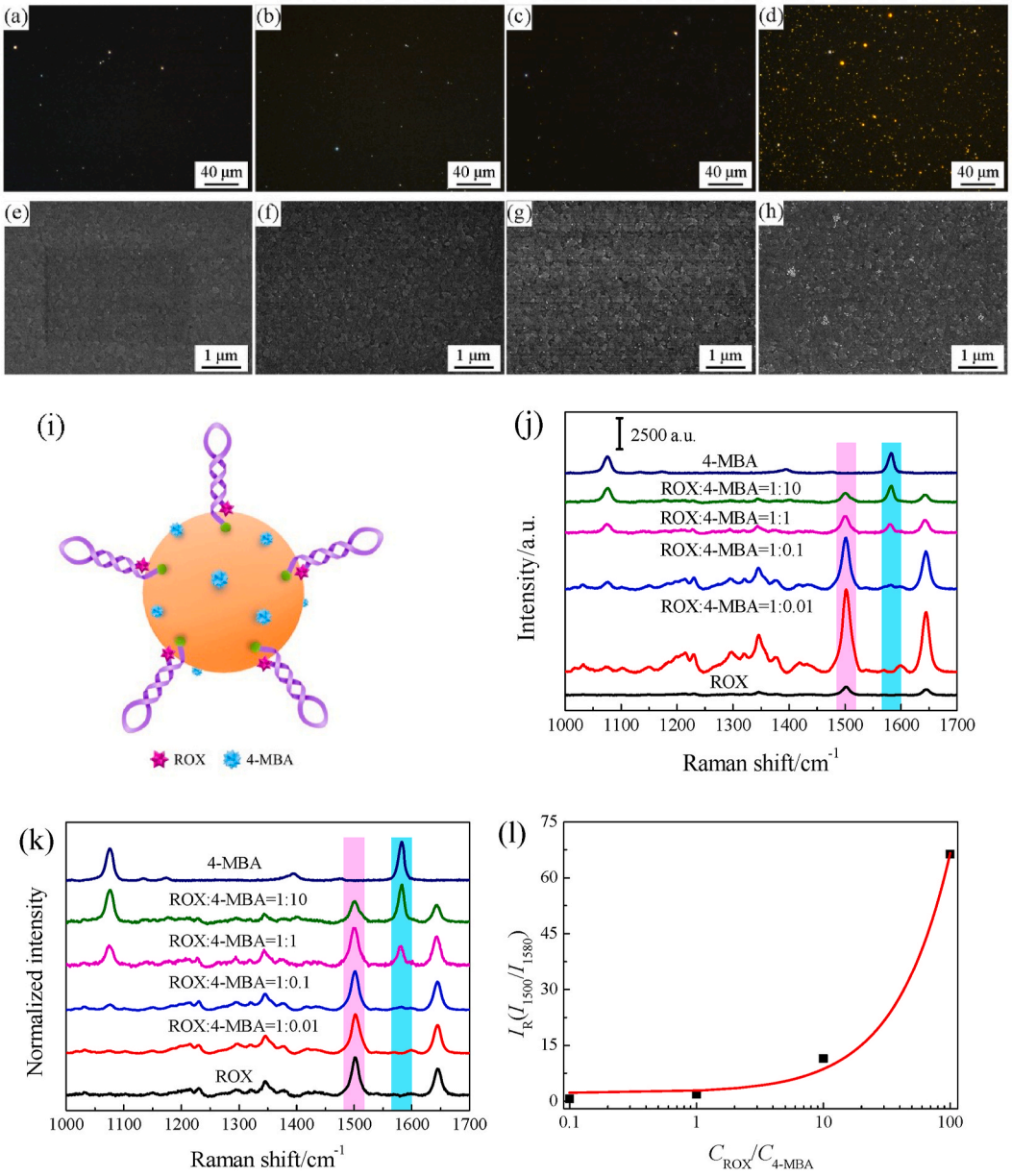

Fig. 3. Feasibility of SPR and ratiometric SERS sensing. (a–h) SPR sensing. DFM and SEM images of (a) and (e) AuNPs, (b) and (f) Probe 2, (c) and (g) blank control, and (d) and (h) the target induced Probe 1-Probe 2 networked structures. (i) Schematic diagram of the ratiometric SERS nanoprobe. (j) SERS spectra obtained from the SERS nanoprobes prepared by different molar ratios of ROX to 4-MBA. (k) Normalized SERS spectra corresponding to the spectra shown in (j). (l) Plots of the SERS intensity ratio of ROX to 4-MBA ($I_R = I_{1500}/I_{1580}$).

Probe 2 affects the formation efficiency of Probe 1-Probe 2 networked structures and the sensitivity of SPR/SERS dual-mode sensing. As shown in Fig. S7, the SPR/SERS sensing strategy was optimized by testing 100 pM miRNA-652 using different dosage ratios of Probe 1 and Probe 2, i.e., 0.5:1, 1:1, 2:1, 3:1, and 5:1, respectively. Figs. S7a–e shows the corresponding sensing results of DFM images, in which the number of yellow spots increases with the increasing dosage ratio of Probe 1 to Probe 2, suggesting the high yield formation of Probe 1-Probe 2 networked structures. Moreover, the corresponding SERS assays were shown in Fig. S7f, in which the SERS spectra were normalized according to the highest intensities at 1500 cm^{-1}. The summarized data of SPR/SERS dual-mode sensing using different dosage ratios of Probe 1 to Probe 2 were plotted in Fig. S7g. With the increasing dosage ratio, an obvious increase in IOD of dark-field color was observed, and the ratiometric SERS was relatively stable when the dosage ratio was up to 1:1, which suggests that the optimal dosage ratio of Probe 1 to Probe 2 can be selected as 1:1.

Incubation time for detecting miRNA-652. In order to investigate the optimal incubation time for target detection, 5 μL of 10 nM miRNA-652 was incubated with Probe 1, Probe 2 and H2 for 30, 60, 90, 120, 150, 180, 210 and 240 min, respectively. Figs. S8a–h shows DFM images of the assays, in which the number of yellow spots increases with the extended incubation time. Fig. S8i shows the normalized SERS spectra of the assay obtained after different incubation times. Fig. S8j plots the summarized assay data of SPR and SERS, which indicates that with the increasing incubation time more Probes 2 were assembled in the networked structures and outputted stronger SERS signal. For SERS assay, the signal reaches a saturation after incubating for 120 min. The IOD-based SPR intensity obviously increased until the incubation time was up to 180 min. In summary, the optimal incubation time of the assay can be selected as 180 min, which is moderate and acceptable relative to that for alternative detection methods (Table S2).

3.6. SPR/SERS dual-mode sensing performance

Under the optimal assay conditions, the performance of the SPR/SERS dual-mode biosensors was characterized by testing miRNA-652 in PBS buffer. Specifically, the biosensors were used to assay 0 (blank), 100 fM, 1 pM, 10 pM, 100 pM, 1 nM and 10 nM miRNA-652 in PBS buffer, respectively. The concentration-related DFM images are shown in Figs. S9a–g and the corresponding IOD-based SPR intensities extracted from the DFM images shown in Fig. 4a follow a linear relationship with the logarithm of miRNA-652 concentration, i.e., I_{SPR} = 50463 × Log C_T +713207 (R^2 = 0.988), and the limit of detection (LOD) is estimated to be 39.2 fM (S/N = 3). Fig. S9h shows the SERS spectra of the assays and the corresponding ratiometric SERS (I_{SERS}= I_{1500}/I_{1580}) values were plotted in Fig. 4b. A linear relationship between the ratiometric SERS and the logarithm of concentration, i.e., I_{SERS} = 0.39 × Log C_T +6.15 (R^2 = 0.996), was obtained and the LOD was 1.48 fM (S/N = 3). The SERS sensing mode has better sensitivity (i.e., SERS mode sensitivity is an order of magnitude higher than the SPR mode), while the SPR sensing mode is more available since it is a label-free detection and acquires the signal just by a simple imaging camera (i.e., it doesn't depend on more sophisticated and expensive instruments like spectrometer and spectral charge coupled device (CCD)). Both the sensing modes show higher or comparable sensitivities relative to the single mode non-gold-nanoparticles-based SERS or SPR detection methods (Table S3). These two sensing modes show complementary advantages, and the combined dual-mode sensing can provide more options for detection and double check the results to improve the accuracy and reliability of the assays.

Fig. 4c and d show the specificity and uniformity characterizations of the SPR/SERS dual-mode biosensors. The specificity was characterized by testing blank sample, specific miRNA-652 (1 pM), and 100 pM unspecific samples (i.e., noncomplementary (UM), three-base mismatch (TM), and single-base mismatch (SM), respectively). Comparing to the specific assay shown in Fig. S10e, almost no yellow dots were observed from the DFM images shown in Figs. S10a–d. Besides, the SERS assay spectra were shown in Fig. S10f. Fig. 4c summarizes the IOD-based SPR intensities and ratiometric SERS values, the sensing signals of mismatched samples are similar to the blank control, which are much lower than the ones of the specific detections. The results demonstrate that the SPR/SERS dual-mode biosensors possess good specificity for miRNA-652 detection. Moreover, according to the specific SERS assay by collecting the SERS spectra from 50 different points, the ratiometric SERS values plotted in Fig. 4d show an appropriate RSD within 12%, indicating the good uniformity of the biosensors.

3.7. Practicability of the SPR/SERS dual-mode biosensors

The practicability of the proposed SPR/SERS dual-mode biosensors was investigated by detecting 0 (blank), 100 fM, 1 pM, 10 pM, 100 pM, 1 nM and 10 nM miRNA-652 spiked in 10% human serum, respectively. Figs. S11a–g shows the DFM images of the assays, and a linear relationship between the IOD-based SPR intensity and the logarithm of miRNA-652 concentration, I_{SPR} = 57640 × Log C_T +825229 (R^2 = 0.984) with LOD of 42.5 fM (S/N = 3), is shown in Fig. 5a. Similarly, Fig. S11h shows the SERS spectra of the assays, and the ratiometric SERS values show a good linear correlation with the logarithm of miRNA-652 concentration ranging from 10 fM to 10 nM (Fig. 5b), i.e., I_{SERS} = 0.48 × Log C_T+7.70 (R^2 = 0.989) with LOD of 2.91 fM (S/N = 3). Both the SPR and SERS are sensitive enough to assay the miRNAs over-expressed in human serum (Geekiyanage et al., 2020; Max et al., 2018). The recovery rate of the proposed SPR/SERS dual-mode biosensor was then investigated by testing 30 fM, 7 pM, and 3 nM miRNA-652 spiked in 10% human serum (Fig. 5c). According to the SERS spectra (Fig. S12a) and DFM images (Figs. S12b–d) of the assays, as well as the above-mentioned SPR (Fig. 5a) and SERS (Fig. 5b) sensing correlation curves, the calculated recoveries of SPR and SERS sensing modes are in the range of 94.67–111.4%, which indicates that the proposed SPR/SERS dual-mode biosensor for miRNA-652 can achieve reliable assay of real samples.

4. Conclusions

In summary, a novel SPR/SERS dual-mode plasmonic biosensor based on CHA-induced AuNP network was proposed to achieve highly sensitive, specific and reliable detection of miRNA-652. The biosensor includes capture DNA-functionalized AuNP (Probe 1), H1 and 4-MBA co-modified AuNP (Probe 2), and fuel strand ROX-labeled H2. In the presence of miRNA-652, target-triggered CHA reactions were executed to induce the formation of Probe 1-Probe 2 networked structures, which

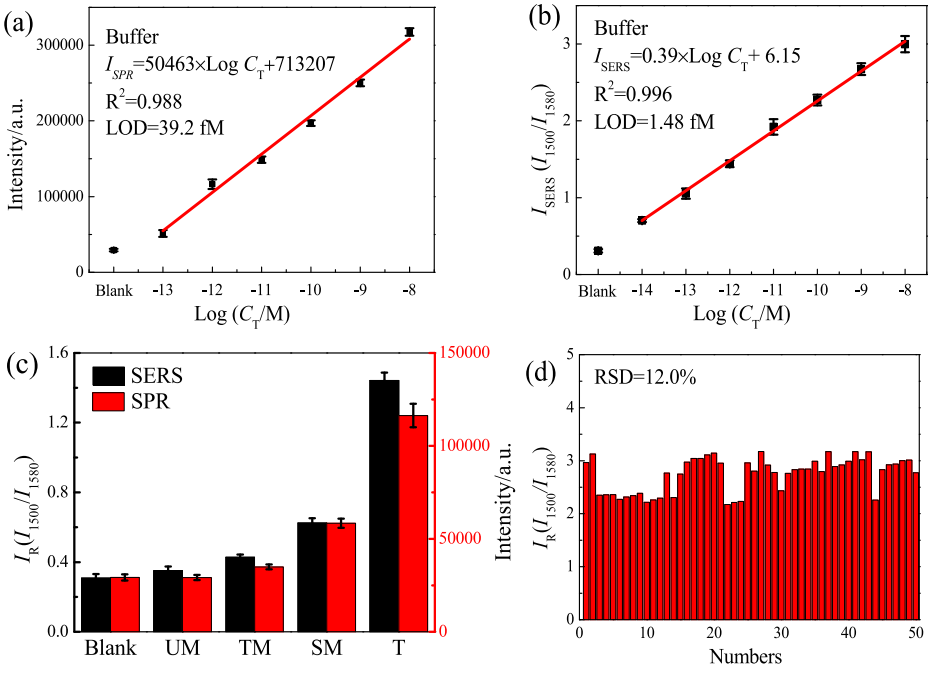

Fig. 4. Performance of SPR/SERS dual-mode sensor. (a) Plots of the integral optical density (IOD) of dark-field color in DFM images (n = 5) and the linear calibration curve of the SPR assay. (b) Plots of the ratiometric SERS (n = 5) and the linear calibration curve of the SERS assay. (c) Histograms of the IOD-based SPR intensity and ratiometric SERS values. (d) Plots of the ratiometric SERS values of the SERS assay recorded from 50 random spots. (For interpretation of the references to color in this figure legend, the reader is referred to the Web version of this article.)

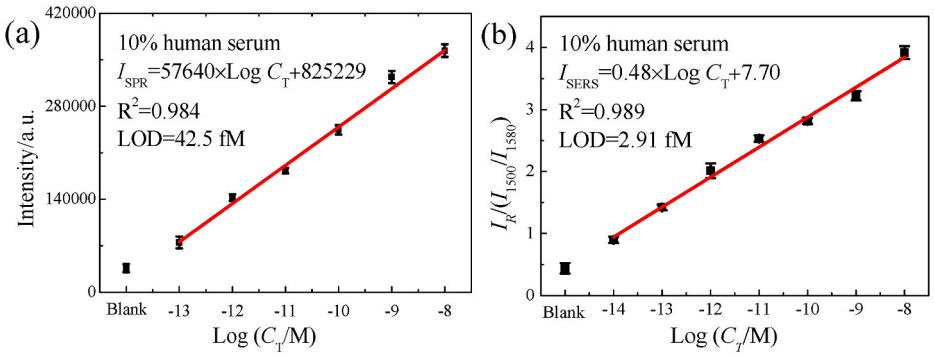

Fig. 5. Practicability of the SPR/SERS dual-mode biosensors. (a) Plots of the integral optical density (IOD) of dark-field color in DFM images (n = 5) and the linear calibration curve of the SPR assay. (b) Plots of the ratiometric SERS (n = 5) and the linear calibration curve of the SERS assay. (c) Recovery rates of the SPR/SERS dual-mode biosensors for miRNA-652 assay. (For interpretation of the references to color in this figure legend, the reader is referred to the Web version of this article.)

(c)

Sample number	Added	Found	Recovery/%	Sensor mode
1	30 fM	28.40 fM	94.67	SERS
		31.22 fM	104.1	SPR
2	7 pM	6.81 pM	97.23	SERS
		7.80 pM	111.4	SPR
3	3 nM	3.14 nM	104.7	SERS
		3.11 nM	103.6	SPR

resulted in the color changes of DFM images and the enhancement of SERS. The SPR sensing mode was achieved by extracting the IOD of dark-field color in the DFM images, and the SERS sensing mode was realized by the ratiometric SERS signals of ROX molecules and the internal standards 4-MBA molecules. The feasibility and sensing mechanism of SPR/SERS dual-mode sensing were confirmed by gel electrophoresis, absorption characterization, SEM and TEM images, DFM images and SERS analyses. The optimal Probe 1/Probe 2 dosage ratio was 1:1, and the preferred incubation time of target detection was 180 min. The proposed SPR/SERS dual-mode sensors possess good performance on sensitivity, specificity, and uniformity. The practicability of the SPR/SERS dual-mode biosensors was confirmed by detecting miRNA-652 in human serum. The SPR mode assay has a linear calibration curve $I_{SPR} = 57640 \times \text{Log } C_T + 825229$ ($R^2 = 0.984$) with LOD of 42.5 fM, and SERS mode assay shows a good linear correlation $I_{SERS} = 0.48 \times \text{Log } C_T + 7.70$ ($R^2 = 0.989$) with LOD of 2.91 fM. The recoveries of SPR and SERS sensing modes were in the range of 94.67–111.4%, which indicates that the proposed SPR/SERS dual-mode biosensor for miRNA-652 can achieve reliable assay of real samples and hold a great application prospect for detection cancer-related nucleic acid markers in early disease screening.

CRediT authorship contribution statement

Chunyuan Song: Conceptualization, Methodology, Formal analysis, Writing – review & editing. **Jingjing Zhang:** Formal analysis, Writing – original draft. **Xinyu Jiang:** Methodology, Investigation. **Hongyu Gan:** Methodology. **Yunfeng Zhu:** Formal analysis. **Qian Peng:** Writing – original draft. **Xinyue Fang:** Methodology. **Yan Guo:** Formal analysis, Data curation. **Lianhui Wang:** Project administration, Supervision.

Declaration of competing interest

The authors declare that they have no known competing financial interests or personal relationships that could have appeared to influence the work reported in this paper.

Acknowledgements

This work was sponsored by the National Key Research and Development Program of China (2017YFA0205300), National Natural Science Foundation of China (61871236), Jiangsu Provincial Key Research and Development Program (BE2018732), Natural Science Foundation of Jiangsu Province of China (BK20181395) and Jiangsu Provincial Qinglan Project.

Appendix A. Supplementary data

Supplementary data to this article can be found online at https://doi.org/10.1016/j.bios.2021.113376.

References

Chen, J., Wu, Y., Fu, C., Cao, H., Tan, X., Shi, W., Wu, Z., 2019. Ratiometric SERS biosensor for sensitive and reproducible detection of microRNA based on mismatched catalytic hairpin assembly. Biosens. Bioelectron. 143, 111619.
Chen, Y., Huang, K., Niu, K., 2018. Recent advances in signal amplification strategy based on oligonucleotide and nanomaterials for microRNA detection-a review. Biosens. Bioelectron. 99, 612–624.
Dyankov, G., Zekriti, M., Bousmina, M., 2012. Dual-mode surface-plasmon sensor based on bimetallic film. Appl. Opt. 51 (13), 2451–2456.
Geekiyanage, H., Rayatpisheh, S., Wohlschlegel, J.A., Brown, R., Ambros, V., 2020. Extracellular microRNAs in human circulation are associated with miRISC complexes that are accessible to anti-AGO2 antibody and can bind target mimic oligonucleotides. Proc. Natl. Acad. Sci. U.S.A. 117 (39), 24213–24223.
Graybill, R.M., Bailey, R.C., 2016. Emerging biosensing approaches for microRNA analysis. Anal. Chem. 88 (1), 431–450.
Guo, J., Keathley, P.D., Hastings, J.T., 2008. Dual-mode surface-plasmon-resonance sensors using angular interrogation. Opt. Lett. 33 (5), 512–514.
He, Y., Yang, X., Yuan, R., Chai, Y., 2019. A novel ratiometric SERS biosensor with one Raman probe for ultrasensitive microRNA detection based on DNA hydrogel amplification. J. Mater. Chem. B 7 (16), 2643–2647.
Hossain, M.K., Kitahama, Y., Huang, G.G., Kaneko, T., Ozaki, Y., 2008. SPR and SERS characteristics of gold nanoaggregates with different morphologies. Appl. Phys. B 93 (1), 165–170.
Lee, K.L., Hung, C.Y., Pan, M.Y., Wu, T.Y., Yang, S.Y., Wei, P.K., 2018. Dual sensing arrays for surface plasmon resonance (SPR) and surface-enhanced Raman scattering (SERS) based on nanowire/nanorod hybrid nanostructures. Adv. Mater. Interfaces 5 (21), e1801064.
Lee, K., Drachev, V.P., Irudayaraj, J., 2011. DNA–gold nanoparticle reversible networks grown on cell surface marker sites: application in diagnostics. ACS Nano 5 (3), 2109–2117.

Li, J., Jiao, Y., Liu, Q., Chen, Z., 2018a. The aptamer-thrombin-aptamer sandwich complex-bridged gold nanoparticle oligomers for high-precision profiling of thrombin by dark field microscopy. Anal. Chim. Acta 1028, 66–76.
Li, J., Liu, Q., Xi, H., Wei, X., Chen, Z., 2017. Y-shaped DNA duplex structure-triggered gold nanoparticle dimers for ultrasensitive colorimetric detection of nucleic acid with the dark-field microscope. Anal. Chem. 89 (23), 12850–12856.
Li, J., Xi, H., Kong, C., Liu, Q., Chen, Z., 2018b. "Aggregation-to-deaggregation" colorimetric signal amplification strategy for Ag(+) detection at the femtomolar level with dark-field microscope observation. Anal. Chem. 90 (19), 11723–11727.
Luo, W., Wu, C., Huang, S., Luo, X., Yuan, R., Yang, X., 2020. Liquid phase interfacial surface-enhanced Raman scattering platform for ratiometric detection of microRNA 155. Anal. Chem. 92 (23), 15573–15578.
Max, K.E.A., Bertram, K., Akat, K.M., Bogardus, K.A., Li, J., Morozov, P., Ben-Dov, I.Z., Li, X., Weiss, Z.R., Azizian, A., Sopeyin, A., Diacovo, T.G., Adamidi, C., Williams, Z., Tuschl, T., 2018. Human plasma and serum extracellular small RNA reference profiles and their clinical utility. Proc. Natl. Acad. Sci. U.S.A. 115 (23), E5334–E5343.
Mocellin, S., Rossi, C.R., Pilati, P., Nitti, D., Marincola, F.M., 2003. Quantitative real-time PCR: a powerful ally in cancer research. Trends Mol. Med. 9 (5), 189–195.
Nguyen, H.H., Park, J., Kang, S., Kim, M., 2015. Surface plasmon resonance: a versatile technique for biosensor applications. Sensors 15 (5), 10481–10510.
Potara, M., Gabudean, A.M., Astilean, S., 2011. Solution-phase, dual LSPR-SERS plasmonic sensors of high sensitivity and stability based on chitosan-coated anisotropic silver nanoparticles. J. Mater. Chem. 21 (11), 3625–3633.
Sauna, Z.E., Kimchi-Sarfaty, C., 2011. Understanding the contribution of synonymous mutations to human disease. Nat. Rev. Genet. 12 (10), 683–691.
Schwarzkopf, M., Pierce, N.A., 2016. Multiplexed miRNA northern blots via hybridization chain reaction. Nucleic Acids Res. 44 (15), e129.
Shu, B., Zhang, C., Xing, D., 2017. A sample-to-answer, real-time convective polymerase chain reaction system for point-of-care diagnostics. Biosens. Bioelectron. 97, 360–368.
Singh, P., 2016. SPR biosensors: historical perspectives and current challenges. Sens. Actuators, B 229, 110–130.
Song, C., Jiang, X., Yang, Y., Zhang, J., Larson, S., Zhao, Y., Wang, L., 2020. High-sensitive assay of nucleic acid using tetrahedral DNA probes and DNA concatamers with a surface-enhanced Raman scattering/surface plasmon resonance dual-mode biosensor based on a silver nanorod-covered silver nanohole array. ACS Appl. Mater. Interfaces 12 (28), 31242–31254.
Taniguchi, M., Miura, K., Iwao, H., Yamanaka, S., 2001. Quantitative assessment of DNA microarrays-comparison with northern blot analyses. Genomics 71 (1), 34–39.
van Rooij, E., Olson, E.N., 2012. MicroRNA therapeutics for cardiovascular disease: opportunities and obstacles. Nat. Rev. Drug Discov. 11 (11), 860–872.
Wang, J., Zhang, R., Ji, X., Wang, P., Ding, C., 2021. SERS and fluorescence detection of circulating tumor cells (CTCs) with specific capture-release mode based on multifunctional gold nanomaterials and dual-selective recognition. Anal. Chim. Acta 1141, 206–213.
Wang, Y., Yan, B., Chen, L., 2013. SERS tags: novel optical nanoprobes for bioanalysis. Chem. Rev. 113 (3), 1391–1428.
Wu, Y., Zhang, Y., Zhang, X., Luo, S., Yan, X., Qiu, Y., Zheng, L., Li, L., 2020. Research advances for exosomal miRNAs detection in biosensing: from the massive study to the individual study. Biosens. Bioelectron. 177, 112962.
Xue, X., Gao, M., Rao, H., Luo, M., Wang, H., An, P., Feng, T., Lu, X., Xue, Z., Liu, X., 2020. Photothermal and colorimetric dual mode detection of nanomolar ferric ions in environmental sample based on in situ generation of prussian blue nanoparticles. Anal. Chim. Acta 1105, 197–207.
Zhang, J., Yang, Y., Jiang, X., Dong, C., Song, C., Han, C., Wang, L., 2019. Ultrasensitive SERS detection of nucleic acids via simultaneous amplification of target-triggered enzyme-free recycling and multiple-reporter. Biosens. Bioelectron. 141, 111402.
Zhang, X.X., Xu, D., Guo, D., Han, H.X., Li, D.W., Ma, W., 2020. Enzyme-free amplified SERS immunoassay for the ultrasensitive detection of disease biomarkers. Chem. Commun. 56 (19), 2933–2936.
Zhang, Y., Shuai, Z., Zhou, H., Luo, Z., Liu, B., Zhang, Y., Zhang, L., Chen, S., Chao, J., Weng, L., Fan, Q., Fan, C., Huang, W., Wang, L., 2018. Single-molecule analysis of microRNA and logic operations using a smart plasmonic nanobiosensor. J. Am. Chem. Soc. 140 (11), 3988–3993.
Zhao, Y., Chen, F., Li, Q., Wang, L., Fan, C., 2015. Isothermal amplification of nucleic acids. Chem. Rev. 115 (22), 12491–12545.
Zong, C., Xu, M., Xu, L.J., Wei, T., Ma, X., Zheng, X.S., Hu, R., Ren, B., 2018. Surface-enhanced Raman spectroscopy for bioanalysis: reliability and challenges. Chem. Rev. 118 (10), 4946–4980.